JOURNAL OF CATALYSIS 149, 100–116 (1994)

Structure and Morphology of Vanadia-Promoted Rh/SiO_2: A Transmission Electron Microscopy Study

B. Tesche,* T. Beutel,† and H. Knözinger†,[1]

*Fritz-Haber-Institut der Max-Planck-Gesellschaft, Faradayweg 4-6, 14195 Berlin, Germany; and †Institut für Physikalische Chemie, Universität München, Sophienstrasse 11, 80333 Munich, Germany

Received January 4, 1994; revised April 15, 1994

Vanadia-promoted Rh/SiO_2-catalysts have been prepared by impregnation followed by calcination at 573, 773, 973, and 1173 K. The structure and morphology of these materials in the oxidized state, and after low (523 K) and high (773 K) temperature reduction, were studied by scanning electron microscopy (SEM), transmission electron microscopy (TEM), microdiffraction, X-ray diffraction (XRD), and CO chemisorption. During calcination at temperatures ≥973 K, a $RhVO_4$ phase is formed, which consists of well-crystallized rod-like particles after calcination at 1173 K. After reduction in H_2, the catalysts consist of highly dispersed Rh° particles as judged from the electron micrographs. This high dispersion is presumably stabilized by interaction of the zerovalent Rh° with the promoter oxide V_2O_3. The well-crystallized sample (calcination at 1173 K) cannot be reduced at 523 K, but at 773 K the rhodium, originally present as $RhVO_4$, is quantitatively reduced to small metal particles in contact with V_2O_3. In contrast to the high dispersion derived from TEM, CO chemisorption gave unexpectedly low CO/Rh ratios, which were even zero for the catalyst calcined at 1173 K. The CO/Rh ratios decreased with increasing calcination temperature ($RhVO_4$ formation) at constant reduction temperature and with increasing reduction temperature at a given calcination temperature. It is suggested that the surface of the highly dispersed Rh° particles is decorated and blocked by VO_x species. This effect, though more pronounced at higher reduction temperature, already occurs after reduction at 523 K. Highly dispersed Rh° particles are produced in the materials studied, particularly when a $RhVO_4$ precursor phase was present, these particles being in intimate contact with a V_2O_3 promoter oxide. In extreme cases (calcination at 1173 K), the encapsulation of Rh° particles seems to be complete, so that no metal surface is exposed. © 1994 Academic Press, Inc.

1. INTRODUCTION

Vanadium-promoted rhodium catalysts have been shown to be highly selective for the synthesis of C_{2+} oxygenates from syngas (1). These catalytic materials, including Rh supported on vanadia (2–4) and Rh/SiO_2 promoted by vanadia (5, 6), have therefore been investigated extensively in the past.

Important factors which seem to determine catalytic activity and selectivity of these materials are the noble metal dispersion and the metal–promoter interaction. The influence of the reduction temperature in rhodium–vanadium systems on the hydrogenation of CO was the subject of several studies (2–9). It has been inferred that the formation of C_{2+} oxygenates favourably proceeds along the metal–promoter perimeter (3, 7–17) where the reactant CO may simultaneously interact with Rh sites and the promoter surface. Mechanistic details of the reaction were recently reviewed in an excellent in-depth article by Hindermann *et al.* (18). Therefore, in attempts to bring the supported components into intimate contact with each other, several synthetic procedures have been developed (19, 20). Kip *et al.* (21) and Hu *et al.* (9) suggested to react suitable precursor compounds so as to form ternary oxide phases which, after reduction, might guarantee good contact between the reduced noble metal component and the promoter oxide or suboxide. High temperature calcination favours the formation of the ternary compound containing rhodium, vanadium and oxygen. The formation of $RhVO_4$ has in fact been reported in the literature for both supported (9, 21–23) and unsupported (24, 25) materials. The work of Hu *et al.* (9) suggested that dispersed metallic rhodium and low-valent vanadium oxide in contact was, in fact, obtained after reduction of the mixed oxide phase. The same research group has also reported on analogous investigations with niobium-promoted rhodium catalysts (26, 27). Legrouri *et al.* (28) have recently reported on the reduction behaviour of $RhCl_3$-impregnated V_2O_5. The reduced phases V_4O_9, VO_2, and V_2O_3 were observed at reduction temperatures of 523, 723, and 873 K, respectively.

We have previously studied the thermal evolution of individual compounds in the temperature range 573–1173 K when $RhCl_3$ and NH_4VO_3 were deposited on SiO_2 as a support (22, 23). The formation of the ternary oxide phase

[1] To whom correspondence should be addressed.

0021-9517/94 $6.00
Copyright © 1994 by Academic Press, Inc.
All rights of reproduction in any form reserved.

$RhVO_4$ could be detected by ^{51}V solid-state NMR (23) and XRD (22) at calcination temperatures of 973 and 1173 K. The reduction behaviour of these materials was also studied (22) by TPR and by IR spectroscopy of chemisorbed CO. The $RhVO_4$ phase could only be reduced in H_2 at temperatures higher than about 520 K. Highly dispersed zerovalent Rh was formed after reduction at 773 K with average particle sizes presumably smaller than 2.5 nm. These particles seemed to be in good contact with a vanadium oxide phase as evidenced by some preliminary transmission electron microscopy (TEM) results (22) and by the fact that a C- and O-bonded CO species could be detected (22) which was assumed to be located at the interface between Rh° particles and the VO_x promoter. To further elucidate the structure and morphology of these materials, we report here a detailed high-resolution transmission electron microscopy (TEM) and scanning electron microscopy (SEM) study. The catalysts were studied in both their oxide precursor state and in the reduced state, with the goal to correlate the characteristics of the final reduced state with the precursor structures as they develop with increasing calcination temperature. For comparison purposes, rhodium-free vanadia on SiO_2 and vanadia-free Rh/SiO_2 had to be included in this investigation. To the best of our knowledge, a systematic study of this kind has not been reported hitherto for this catalyst system.

2. EXPERIMENTAL

2.1. Catalyst Preparation

Preparation procedures were the same as described earlier (22). The rhodium catalysts were prepared by impregnation of the silica support (SiO_2, Alpha Products, 340 m^2/g) with a methanol solution of $RhCl_3 \cdot 3H_2O$ (Johnson-Matthey). The solvent was evaporated at 310 K at a pressure of approximately 2.5 kPa. The impregnated support was then dried for 12 h at 383 K and ground in an agate mortar prior to calcination in air at 573, 773, 973, and 1173 K. These materials are denoted Rh/573, Rh/773, Rh/973, and Rh/1173, respectively, their nominal metal loading being 3.8 wt% Rh.

Vanadia supported on silica was made by impregnation of the silica with an aqueous solution of NH_4VO_3. The calculated vanadium loading was 6.5 wt%. The precursor was decomposed by heating the samples in air for 3 h at 773 K. Subsequent calcination in air for 7 h at 573, 773, 973, and 1173 K gave four samples denoted V/573, V/773, V/973, and V/1173.

The preparation of the vanadium-oxide-promoted rhodium catalysts was carried out by impregnation of NH_4VO_3/SiO_2 after decomposition at 773 K with $RhCl_3 \cdot 3H_2O$ in the same way as described for the pure rhodium catalysts. The resulting samples are denoted Rh/V/573, Rh/V/773, Rh/V/973, and Rh/V/1173. They formally contain 3.3 wt% Rh and 6.8 wt% V, corresponding to an atomic ratio V : Rh equal to 4.2.

Reduction of the materials was carried out in a flow (50 cm^3/min) of H_2 (Linde 5.0) for 1 h at either 523 K (low temperature reduction, LTR) or 773 K (high temperature reduction, HTR). The reduced materials were stored in sealed ampoules under dry N_2 until use for electron microscopy.

2.2. Transmission Electron Microscopy (TEM)

For TEM investigations, the powder materials were placed onto a specially prepared, structureless carbon film with a thickness of 4 nm. These thin films are sufficiently stable for covering Cu grids of 60 μm mesh width, the additional use of holey organic films not being necessary. The catalyst powders were suspended in ethanol ultrasonically, and a drop of the resulting suspension was deposited on the carbon film. The remaining solvent was removed after 1 min.

The electron microscopy was carried out on a Siemens Elmiskop 102 operated at 100 kV. An electron-optical magnification of 120,000 : 1 and a diffraction length of 700 mm were sufficient to extract all significant structural and morphological details. The diffraction length was calibrated with thallium chloride.

The distributions of particle sizes was approximated by a Gaussian function, which was fitted to the data points by a least-squares fit.

2.3. Scanning Electron Microscopy (SEM)

For SEM, the materials were mounted onto beryllium disks. They were then examined in a Hitachi 4000 microscope without the usual sputter deposition of a gold film. The microscope was equipped with a cold field emission gun operated at 15 kV. The spatial resolution was approximately 10 nm. Elemental compositions of the samples were analyzed by energy-dispersive X-ray analysis (EDX).

2.4. X-Ray Diffraction (XRD)

A transmission goniometer Siemens type D 500 with Guinier focussing and equipped with a position-sensitive proportional counter was used for XRD. The applied CuK_α radiation (40 kV, 25 mA) was monochromatized with a Ge(111) crystal.

2.5. CO Chemisorption

In preparation for dispersion measurements, catalyst samples were treated in flowing O_2 (100 ml/min) at 573 K for 20 min so as to remove hydrocarbon contamination. They were then reduced in flowing H_2 (50 ml/min) by

heating at a rate of 5 K/min up to 523 or 773 K, at which temperatures the samples were held for one hour. Subsequently, the samples were purged with N_2 for 15 min at the respective reduction temperature and cooled to 300 K in flowing N_2. The prereduced catalysts were sealed under N_2 in glass vials and stored until use for CO chemisorption.

The CO uptakes were determined by the "pulse flow" method using a Micromeritics Pulse Chemisorb 2700 apparatus. Approximately 50 mg of the prereduced catalysts were transferred to the adsorption tube in air and then brought to 473 K at a heating rate of 30 K/min in flowing H_2 (20 ml/min) and reduced *in situ* for 30 min. Chemisorption of CO was measured at 300 K by repeated injection of 70 μl volumes of CO into H_2 carrier gas (20 ml/min) until saturation was reached. the limits of detectability of the chemisorption under the conditions used were approximately 3–4 μg CO per g catalyst.

3. RESULTS AND DISCUSSION

3.1. Oxidized Samples

3.1.1. Silica. For comparison, Fig. 1 shows an electron micrograph of the pure support SiO_2 after thermal treatment in air at 573 K. Consistent with the high surface area of the SiO_2 of 340 m^2/g, the micrograph shows irregularly formed particles which appear to be interconnected and which have typical dimensions of 20–40 nm.

3.1.2. Vanadia on SiO_2. The electron micrographs of V/573 and V/1173 are compared in Figs. 2a and 2b. The appearance of sample V/573 is very similar to that of the pure SiO_2 support, although the NH_4VO_3 should have been decomposed and at least partially converted into V_2O_5 at 573 K and although the surface area of the material was decreased relative to the pure support from 340 to 226 m^2/g (22). It appears that the VO_x phase should be highly dispersed in this sample. The sintering of the material continued at increasing temperature (22), and this becomes clearly evident from the micrograph of sample V/1173 in Fig. 2b which shows a gigantic particle having rounded edges. At this stage, the surface area has decreased to 12 m^2/g. At certain locations along the edges, fringes can be seen which are documented by 2 to 10 dark lines being parallel to each other and to the surface of the large particle. One of these areas is shown in Fig. 3 at enhanced magnification. The fringes can now be seen clearly and a stacking fault (denoted SF) in the docu-

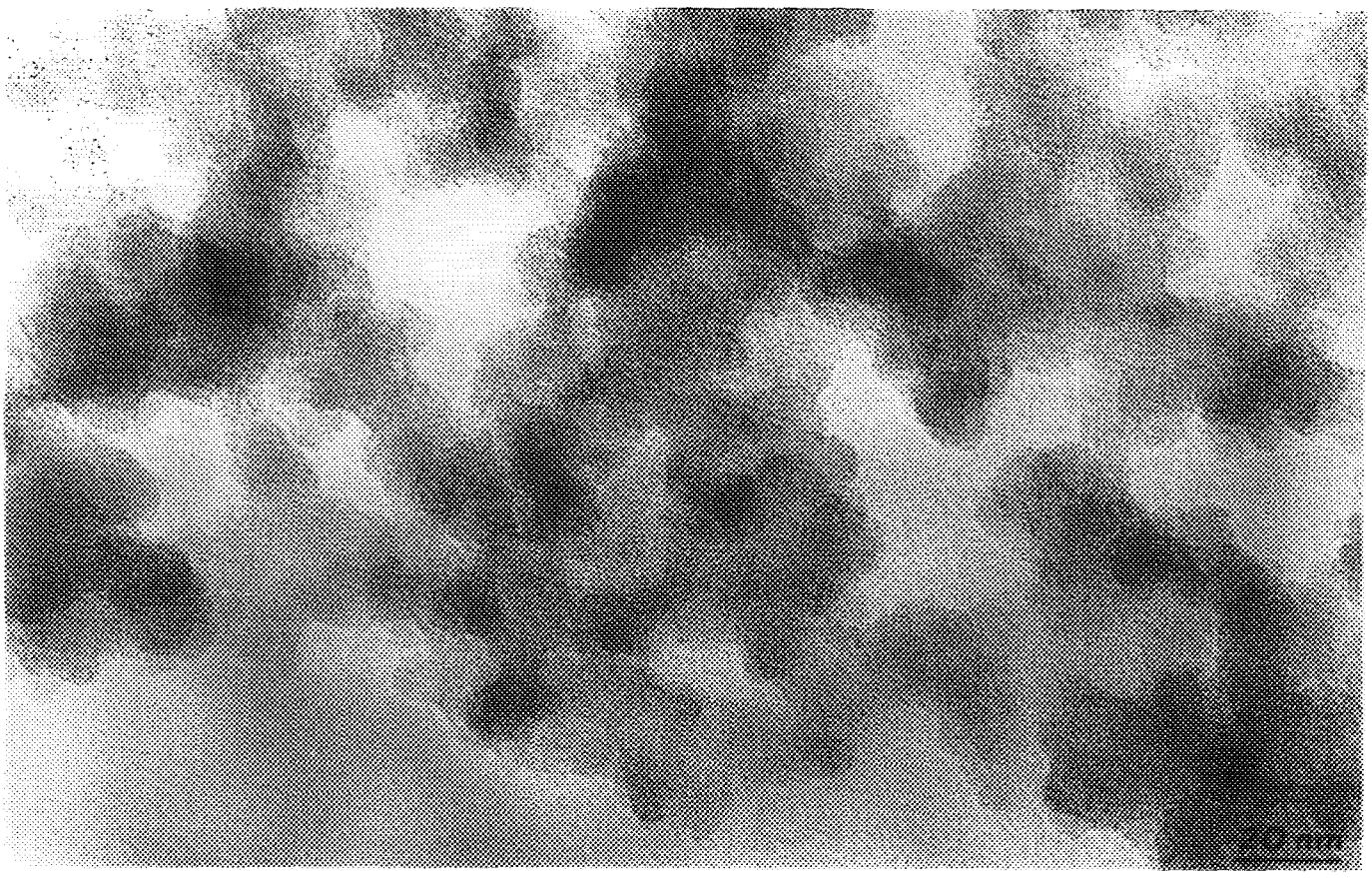

FIG. 1. Transmission electron micrograph of the SiO_2 support.

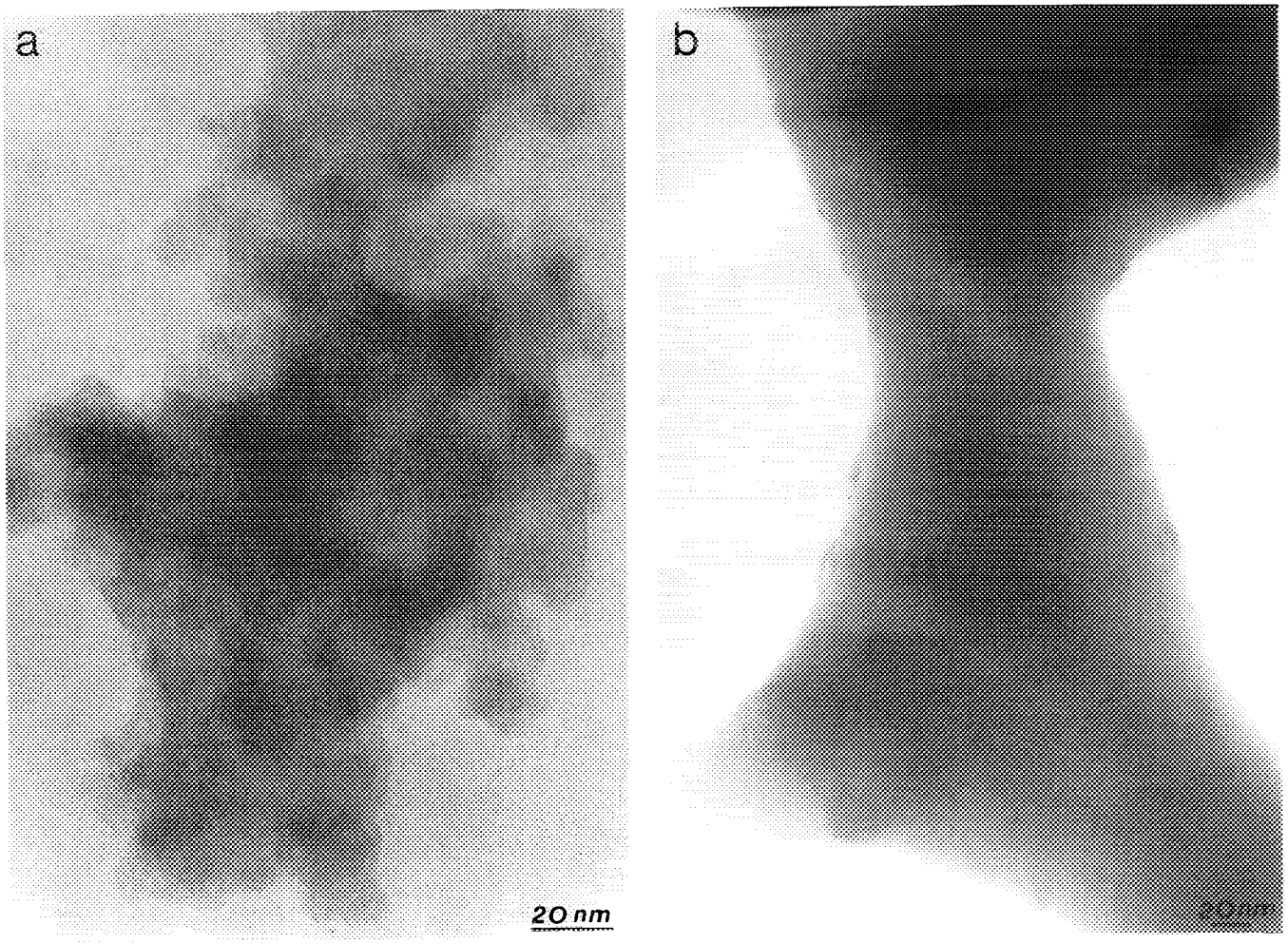

FIG. 2. Transmission electron micrographs of (a) sample V/573 and (b) sample V/1173.

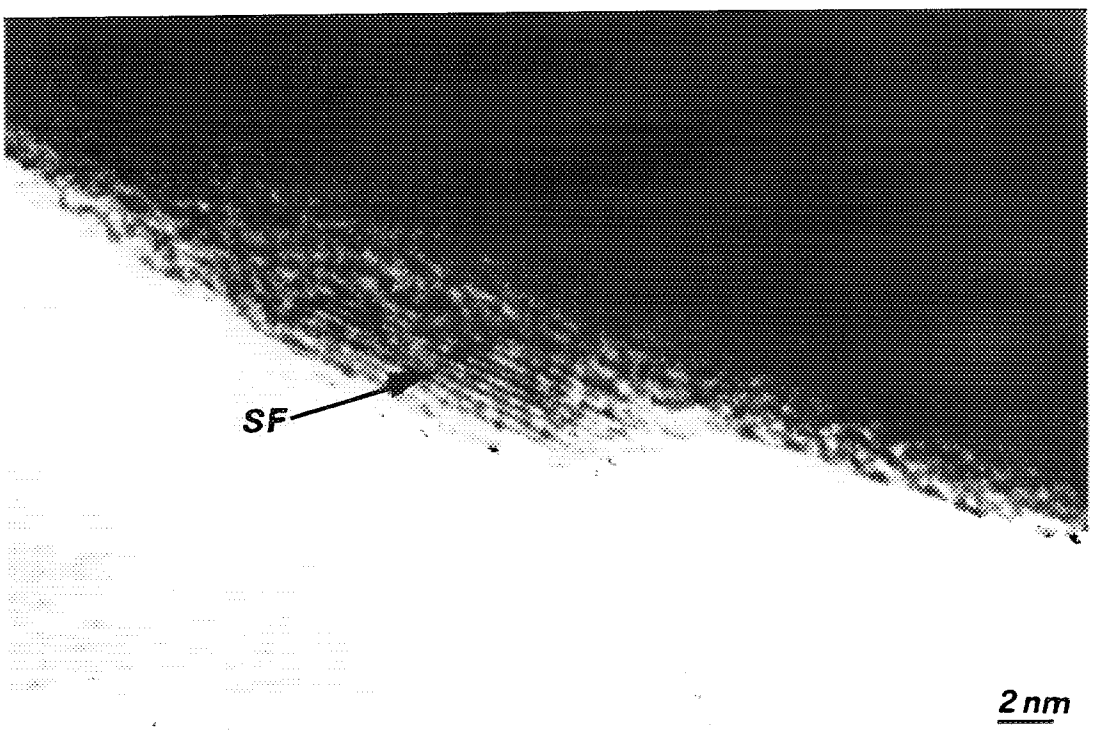

FIG. 3. Area of micrograph (b) in Fig. 2 of sample V/1173 showing characteristic lattice fringes of V_2O_5.

mented structure is also observed. The spacings between the fringes are 0.43 nm and are consistent with the presence of small islands of three-dimensional V_2O_5 with its (001) plane being oriented parallel to the underlying silica surface.

The sintering of the SiO_2 is obviously induced by the presence of V_2O_5 in the samples which acts as a flux since the surface area of pure SiO_2 only decreases to 250 m^2/g on calcination at 1173 K. Similar phenomena with BET surface areas decreasing by an order of magnitude were observed by del Arco *et al.* (29), when vanadium-oxide-containing materials were calcined at temperatures between 973 and 1173 K. The sintering may be induced by condensation of V_2O_5 (m.p. 963 K) into the silica pores and/or narrow interparticle space.

The vanadium distribution in the samples is not homogeneous. This can be seen in the SEM picture of sample V/1173 shown in Fig. 4. Large particles are evident and EDX (see inset) demonstrates that vanadium is clearly present in or on these particles. In contrast, much less vanadium was detected in areas which showed agglomerates of smaller, lengthy particles having typical dimensions of 500–1000 nm in length and approximately 200 nm in width. This observation is consistent with the assumption that the sintering phenomenon is strongly dependent on the presence of V_2O_5 as a flux.

3.1.3. Rhodium on SiO_2. Figure 5 shows micrographs of Rh/573, Rh/773, and Rh/1173. The appearance and morphology of the SiO_2 support does not significantly vary in this set of micrographs and is very similar to that of pure SiO_2 (see Fig. 1). This is consistent with a comparably small loss in surface area with increasing calcination temperature. In fact, the surface of Rh/1173 (263 m^2/g) is practically identical to that of pure SiO_2 (251 m^2/g) when calcined at the same temperature (22). In the micrograph of sample Rh/573 (Fig. 5a), small particles in a bimodal distribution in the size ranges between 0.3 and

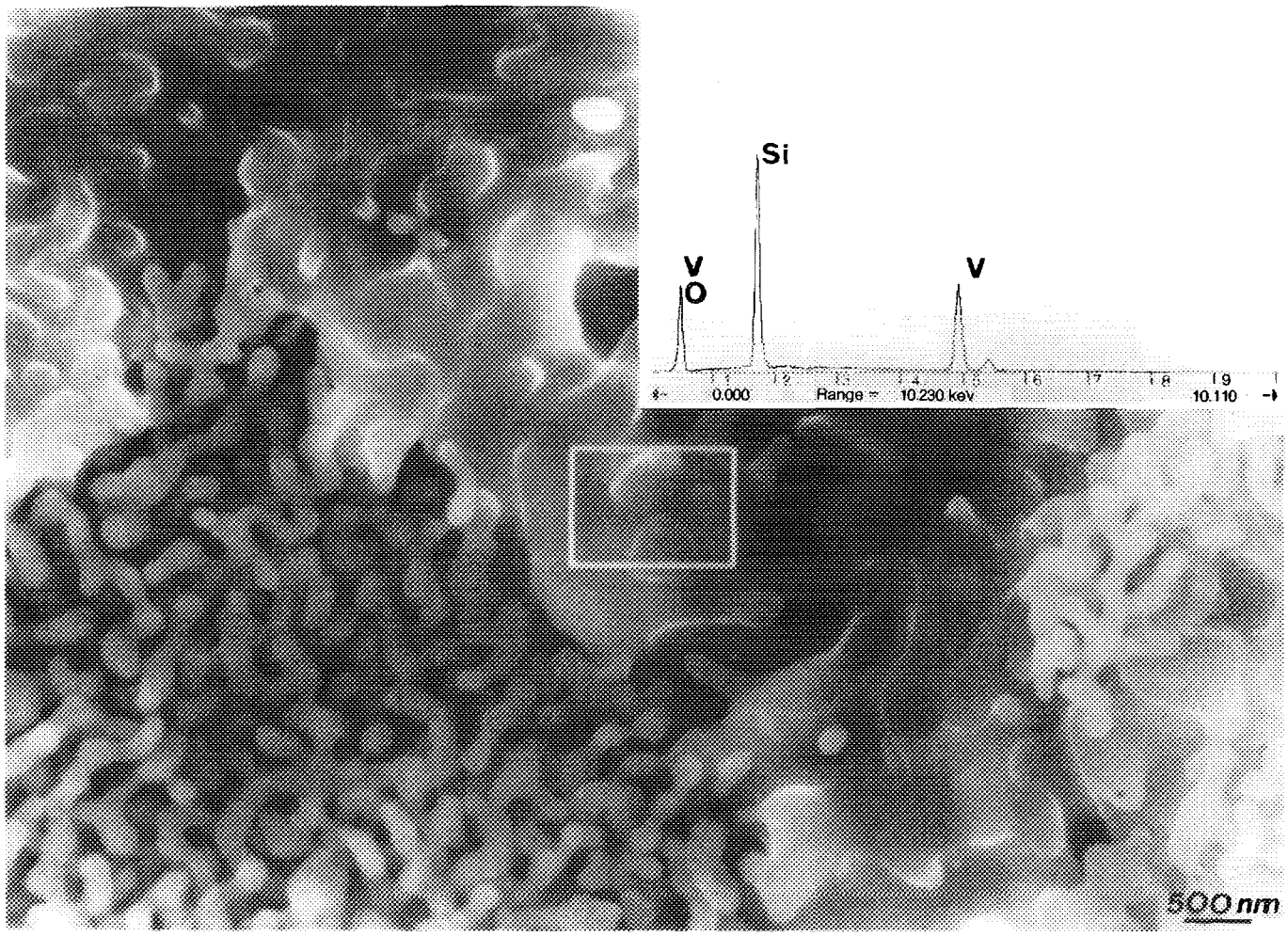

FIG. 4. Scanning electron micrograph of sample V/1173.

0.7 nm and between 1.0 and 2.6 nm can be recognized. These must correspond to $RhCl_3$ crystallites in high dispersion, since Rh_2O_3 is not formed at this low temperature (22). Consistent with earlier XRD results (22), disperse α-Rh_2O_3 is formed in sample Rh/773 as indicated by the observation of particles in Fig. 5b which have diameters of ca. 1.5–2.0 nm. Significant particle growth is evident in Fig. 5c, which shows the micrograph of Rh/1173. The large particles of α-Rh_2O_3 have dimensions of 20–30 nm this being in very good agreement with the average particle size of 30 nm as determined by XRD (22). Some of the particles seem to have rod-like morphologies besides the dominent globular particles and indications of developing crystal planes are seen.

The observed growth of Rh_2O_3 particles with increasing temperature of calcination is consistent with the TEM results reported by Yates and Sinfelt (30) for a similar catalyst system. Analogous results were reported by Duprez *et al.* (31), and Chen *et al.* (32) observed a significant increase in mean Rh_2O_3 particle size when a Rh film deposited on a planar, amorphous silica model support was oxidized and thermally treated at temperatures above 873 K.

3.1.4. Rhodium on vanadia/SiO_2. Figure 6 shows characteristic micrographs of samples Rh/V/573, Rh/V/773, and Rh/V/973. The appearance of the vanadia-containing silica support material of Rh/V/573 and Rh/V/773 in Figs. 6a and 6b, respectively, closely resembles that of the vanadia-free samples in Figs. 5a and 5b. However, the $RhCl_3$ and Rh_2O_3 particles in Rh/V/573 and Rh/V/773, respectively, as indicated by the dark spots are smaller than in the corresponding vanadia-free samples. Average diameters are approximately 1 nm, consistent with the fact that they were not detectable by XRD (22). As in the case of V/573 (Fig. 2a) and V/773, VO_x particles are not visible in the micrographs, although the formation of V_2O_5 crystallites was detected by XRD (22). The results suggest that the presence of vanadia has a dispersing effect on the rhodium compounds at these low calcination temperatures.

The surface area only decreased by approximately 16% for Rh/V/973 (160 m^2/g) relative to Rh/V/773 (190 m^2/g). Consequently, significant sintering is not seen in the micrograph of sample Rh/V/973 (Fig. 6c). The Rh_2O_3 undergoes particle growth at the calcination temperature of 973 K, indicated by somewhat larger spots in the micrograph (average size 3.0 nm) as compared to those observed for Rh/V/773 in Fig. 6b. In addition, still larger rounded particles are visible, which most probably have to be attributed to $RhVO_4$ which was detectable by XRD (22). Their dimensions are typically 20–40 nm.

The $RhVO_4$ phase is undoubtedly formed when the material is calcined at 1173 K. The X-ray diffractogram of Fig. 7 is clearly dominated by the signature of this phase. The measured *d*-spacings and crystallographic *a*- and *c*-values are summarized and compared with those reported in the literature in Tables 1 and 2, respectively. Figure 8 is a SEM picture of sample Rh/V/1173. The strong sintering which was observed for the corresponding rhodium-free material V/1173 (Fig. 2b) is obvious also in this sample and the X-ray diffractogram of Fig. 7 indicates that some

TABLE 1

X-Ray Diffraction Data for $RhVO_4$ Supported on Silica

Oxidized samples					H_2 treated at 523 K	
Ref. (9)		Present XRD		TEM	XRD	TEM
d (nm)	I/I_0	*d* (nm)	I/I_0	*d* (nm)	*d* (nm)	
					0.325	
0.3223	100	0.3235	100			
						0.316
				0.310		
						0.291
					0.253	
		0.2491	14			
0.2489	54	0.2461	67		0.246	
0.2272	20	0.228	20			
					0.222	
0.2182	17	0.2167	15			
				0.215		0.215
0.2038	13	0.2046	9			
		0.1949	8			
		0.1882	6			
				0.179	0.173	
0.1678	50	0.1674	54			
					0.166	
0.1609	18	0.1616	20			
0.1489	13					
		0.1459	13			
		0.1445	15			
0.1438	15	0.1437	7			
0.1350	22	0.1350	19			
		0.1330	15			
0.1245	11	0.1230	9			

TABLE 2

Crystallographic Parameters of Unsupported and Silica-Supported Tetragonal $RhVO_4$

$RhVO_4$	*a* (nm)	*c* (nm)	Ref.
Unsupported	0.455	0.291	(25)
	0.465	0.301	(24)
Supported	0.4567	0.2916	(22)
	0.4558	0.2971	(9)
	0.4582	0.292	Present study

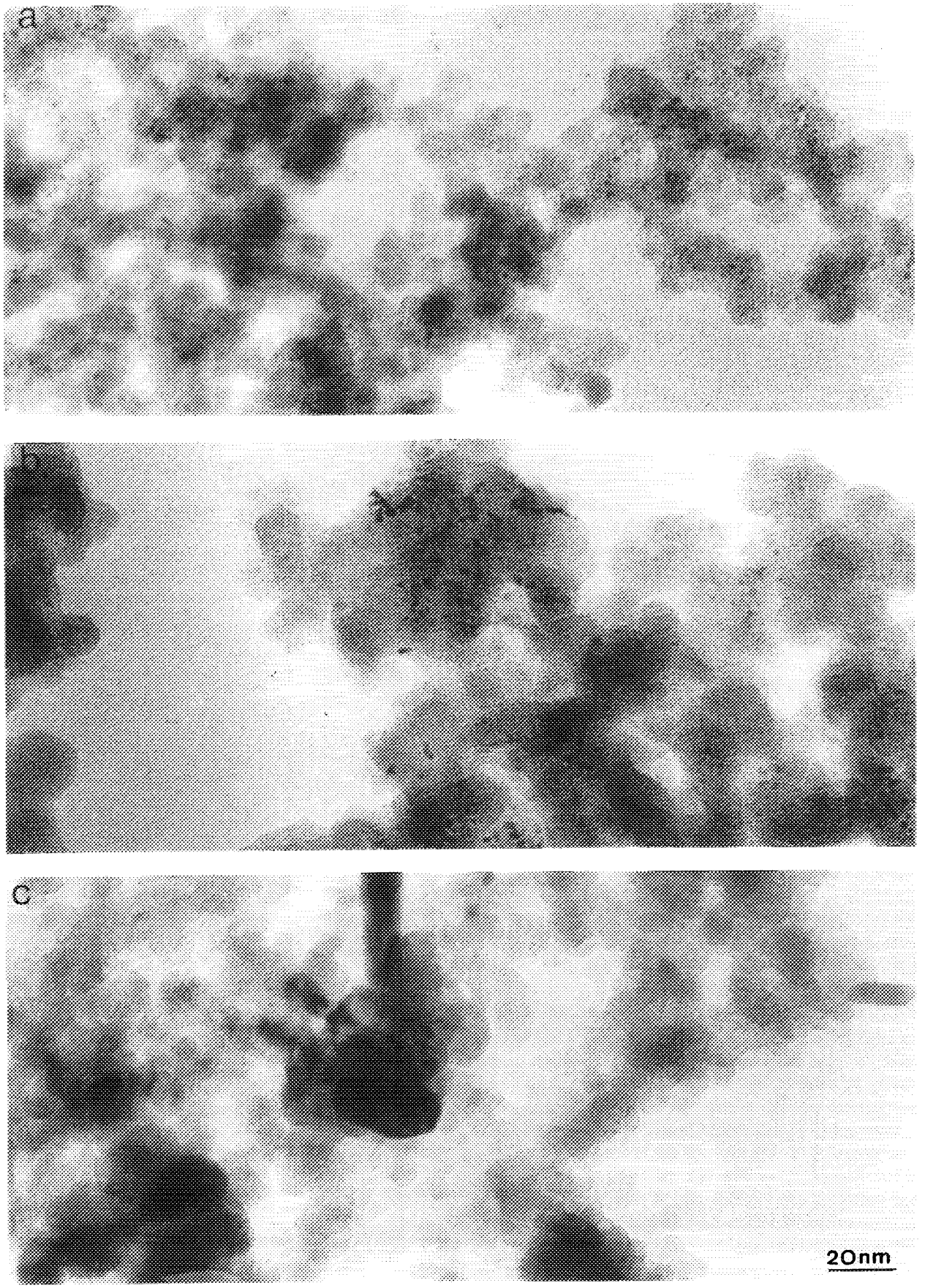

FIG. 5. Transmission electron micrographs of (a) sample Rh/573, (b) sample Rh/773, and (c) sample Rh/1173 in their oxide precursor state.

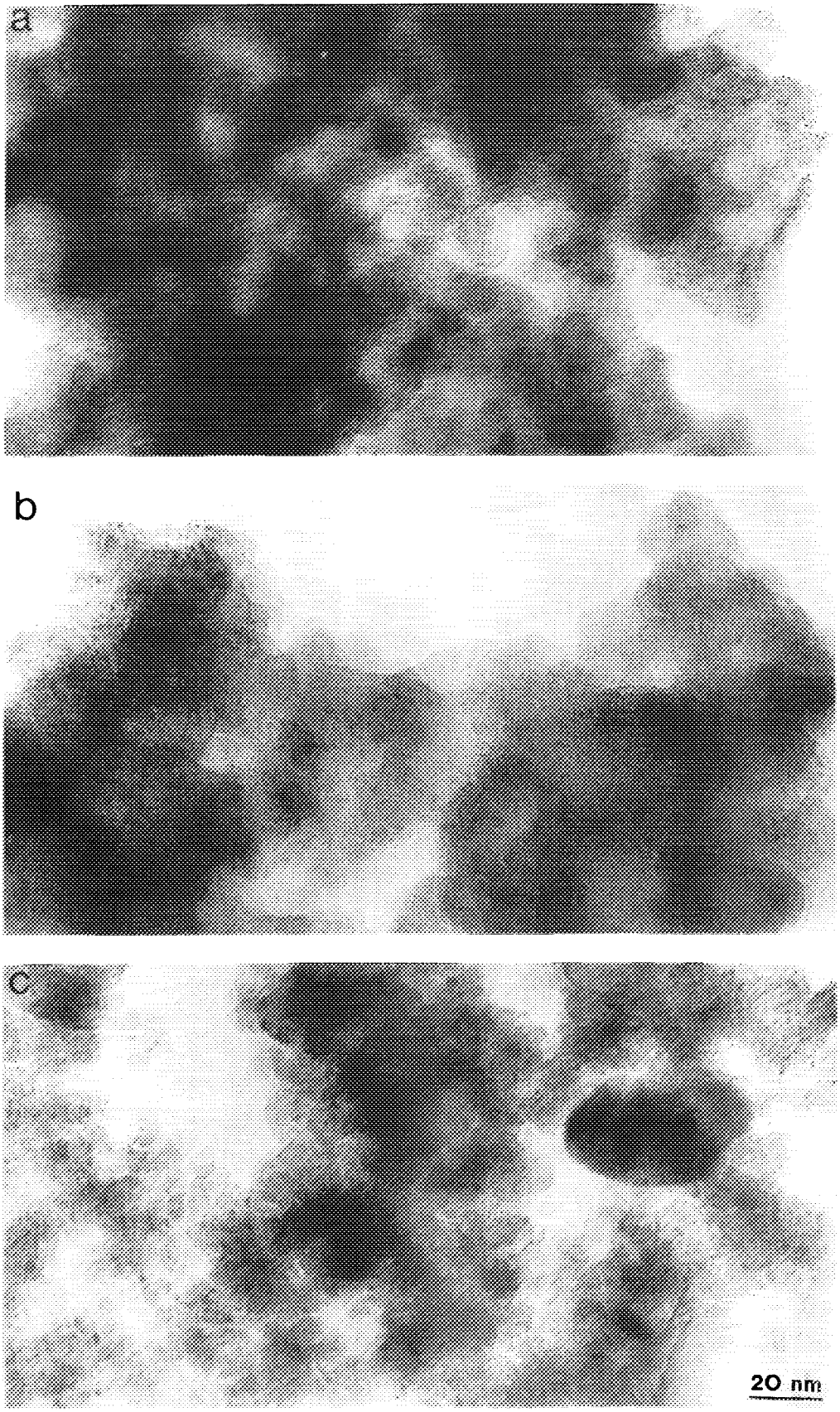

FIG. 6. Transmission electron micrographs of (a) sample Rh/V/573, (b) sample Rh/V/773, and (c) sample Rh/V/973 in their oxide precursor state.

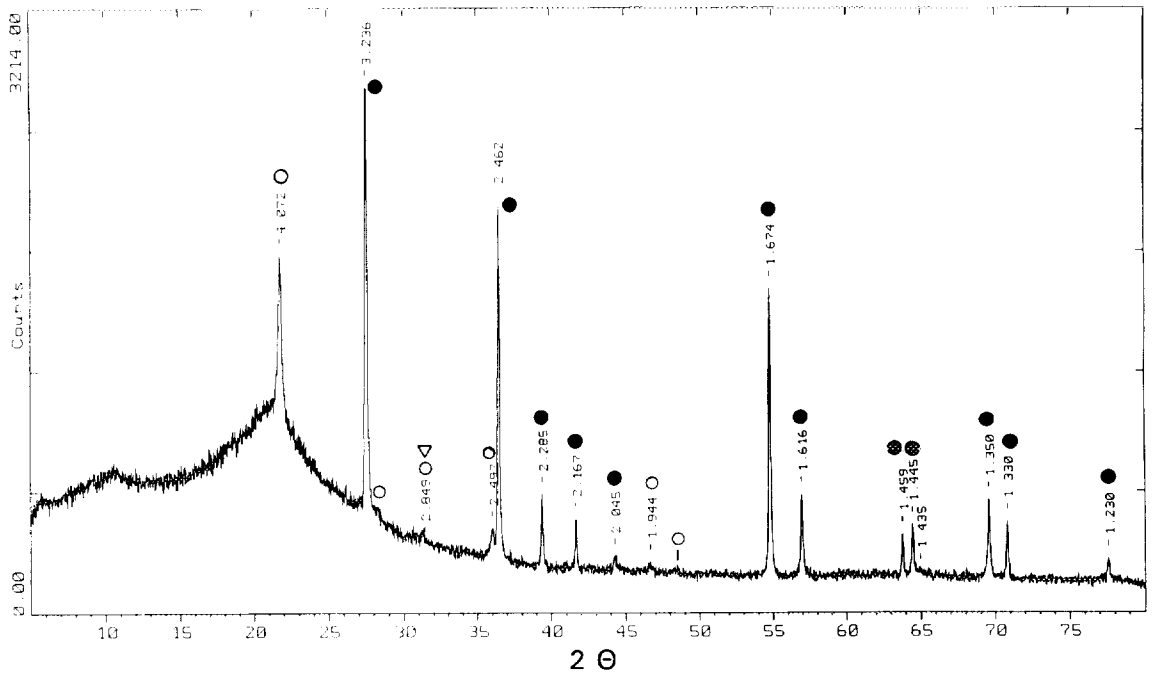

FIG. 7. X-ray diffraction pattern of sample Rh/V/1173: (●) $RhVO_4$, (○) α-cristobalite, and (▽) V_2O_5.

cristobalite particles have also formed. In addition, rod-like particles are seen, which have typical lengths between 50 and several hundred nm and widths of 20–200 nm. A few larger crystallites are shown in the central part of the SEM picture in Fig. 8. An EDX analysis (inset in Fig. 8) of this area shows the presence of oxygen, vanadium, and rhodium consistent with the attribution of these features to the $RhVO_4$ phase, although the stoichiometry of these

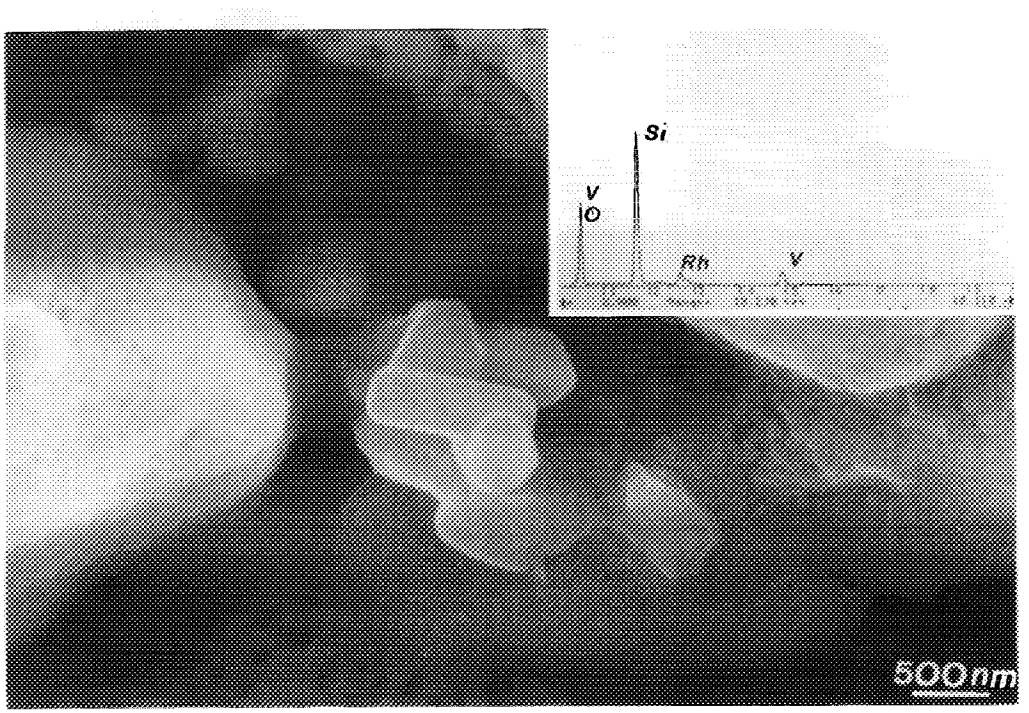

FIG. 8. Scanning electron micrograph of sample Rh/V/1173.

crystallites could not be determined with sufficient accuracy by our EDX analysis.

The micrographs of Fig. 9 provide further support for this assignment. The micrographs of Figs. 9a and 9b clearly show several, though smaller, rod-like structures located on the surface of large silica (cristobalite) particles. An individual crystallite is demonstrated in Fig. 9c and a microdiffraction pattern of this particle is shown in the inset. The three *d*-spacings that can be extracted from the microdiffraction are included in Table 1. They do not coincide well with spacings found in XRD within the limits of accuracy of the TEM-derived *d*-values. However, the *d*-value at 0.179 nm is close to a value found by in situ XRD for samples which are treated in flowing H_2 at 523 K (see Table 1). This suggests that the microcrystals undergo some unknown structural transformation in the electron flux in the electron microscope.

3.2. Reduced Samples

3.2.1. Vanadia on silica. X-ray diffraction did not give any indication of a crystalline vanadium-containing phase when the samples were reduced at 523 K, while reduction at 773 K suggested the formation of V_2O_3 (22). These results are in perfect agreement with the appearance of reduced vanadia on silica samples in the electron micrographs (not shown). The morphologies of the reduced samples very closely resemble those of the oxidized precursor materials. With V/1173 reduced at 773 K, fringes can be seen in addition to small dark flecks. Both features are most probably to be attributed to the presence of V_2O_3.

3.2.2. Rhodium on silica. Figures 10a and 10b show micrographs of samples Rh/573 and Rh/1173, respectively, after H_2-reduction at 523 K. The Rh° particles seen in Fig. 10a of Rh/573 cover a wide particle size range between 0.5 and 5 nm, as shown in the histogram of Fig. 11a. This size distribution is a consequence of the high dispersion of the precursor $RhCl_3$ particles prior to reduction (see Section 3.1.3). In contrast, the reduced sample Rh/1173 contains a few large Rh° particles as shown in Fig. 10b, which have typical dimensions of 10–30 nm consistent with the average particle diameters of 11 nm obtained from XRD linewidths (22). The formation of these large Rh° particles relates to the dimensions of the α-Rh_2O_3 particles in the oxidized precursor state (see Section 3.1.3) (22).

3.2.3. Rhodium on vanadia/SiO_2. As reported earlier (22), Rh/V/1173 cannot be reduced at 523 K. Figures 12a–12c therefore only show the electron micrographs of samples Rh/V/573, Rh/V/773, and Rh/V/973 after reduction in H_2 at 523 K. Rather small spots, which are uniform in size (approximately 0.55–0.7 nm), are seen in Fig. 12a of sample Rh/V/573. These Rh° particles are significantly smaller on average and show a much narrower size distribution than those found for the corresponding vanadium-free material (see Fig. 11a). This is probably due to the strong interaction between Rh° and presumably V_2O_3. The high dispersion of Rh° in this sample is consistent with the observation of the gem-dicarbonyl species in the FTIR spectra of chemisorbed CO (22).

The Rh° particles formed on reduction on Rh/V/773 (Fig. 12b) are larger than those observed for Rh/V/573 and gave the size distribution shown in Fig. 11b. The most abundant particles have diameters of 1.7 nm; the average particle size is 1.8 nm. In Rh/V/973 the formation of $RhVO_4$ had already started (22) and was apparent in the micrograph of Fig. 6c as large rounded particles with dimensions of 20–40 nm (see Section 3.1.4). When this material was reduced at 523 K, micrographs as shown in Fig. 12c were obtained. Large patches of sizes and morphologies similar to those observed on the oxide precursor can be recognized, which in their reduced state are now decorated by a large number of very small and uniform spots. These are interpreted as highly dispersed Rh° resulting from the reduction of the $RhVO_4$ phase. This reduction process is probably nucleation controlled, thus leading to the large number of metal particles which are stabilized by strong interaction with the remaining partially reduced oxide matrix. The highly dispersed Rh° metal particles have dimensions between 0.5 and 0.9 nm.

When Rh/V/1173 was treated in H_2 at 523 K, characteristic micrographs were obtained (Fig. 13a) which are almost identical to those of the oxide precursor. Figure 13a shows the rod-like particles which had been identified as $RhVO_4$ in the oxide sample (see Section 3.1.4). The microdiffraction pattern of these particles after H_2 treatment at 523 K is shown in the inset in Fig. 13a, and the *d*-spacings calculated from this pattern are included in Table 1 and compared to those obtained from X-ray diffraction of a corresponding sample. There is obviously no close correspondence between the *d*-spacings measured by the two techniques, again suggesting that structural transformations are probably induced by the electron bombardment in the electron microscope. It is interesting to note that the diffractogram of the H_2-treated sample (see Table 1) although reduction was not detected at 523 K differs from those of the original calcined materials. Indications for structural modifications under comparable conditions had been recognized previously (22), and Hu *et al.* (9) reported the observation of an unidentified phase besides $RhVO_4$ after H_2-treatment at 473 K.

The micrograph of Fig. 13a does not show any indication of Rh° metal particles, consistent with the irreducibility of Rh/V/1173 at 523 K.

Figure 13b shows two typical micrographs obtained when Rh/V/1173 was reduced at 773 K. Structures can be seen which are still similar in size and morphology to the rod-like particles in the oxide precursor material

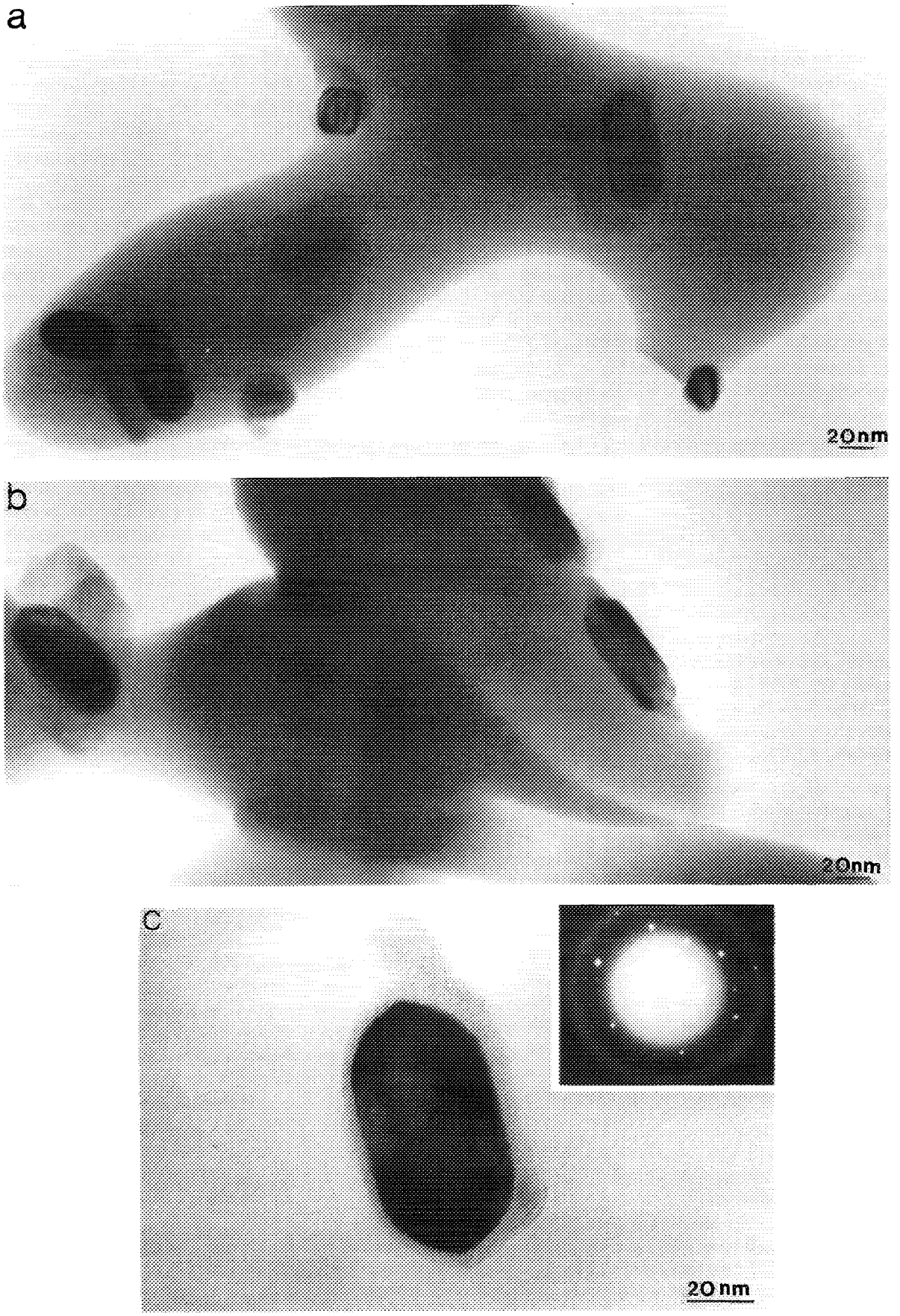

FIG. 9. Transmission electron micrographs of three different areas of sample Rh/V/1173 in the oxide precursor state.

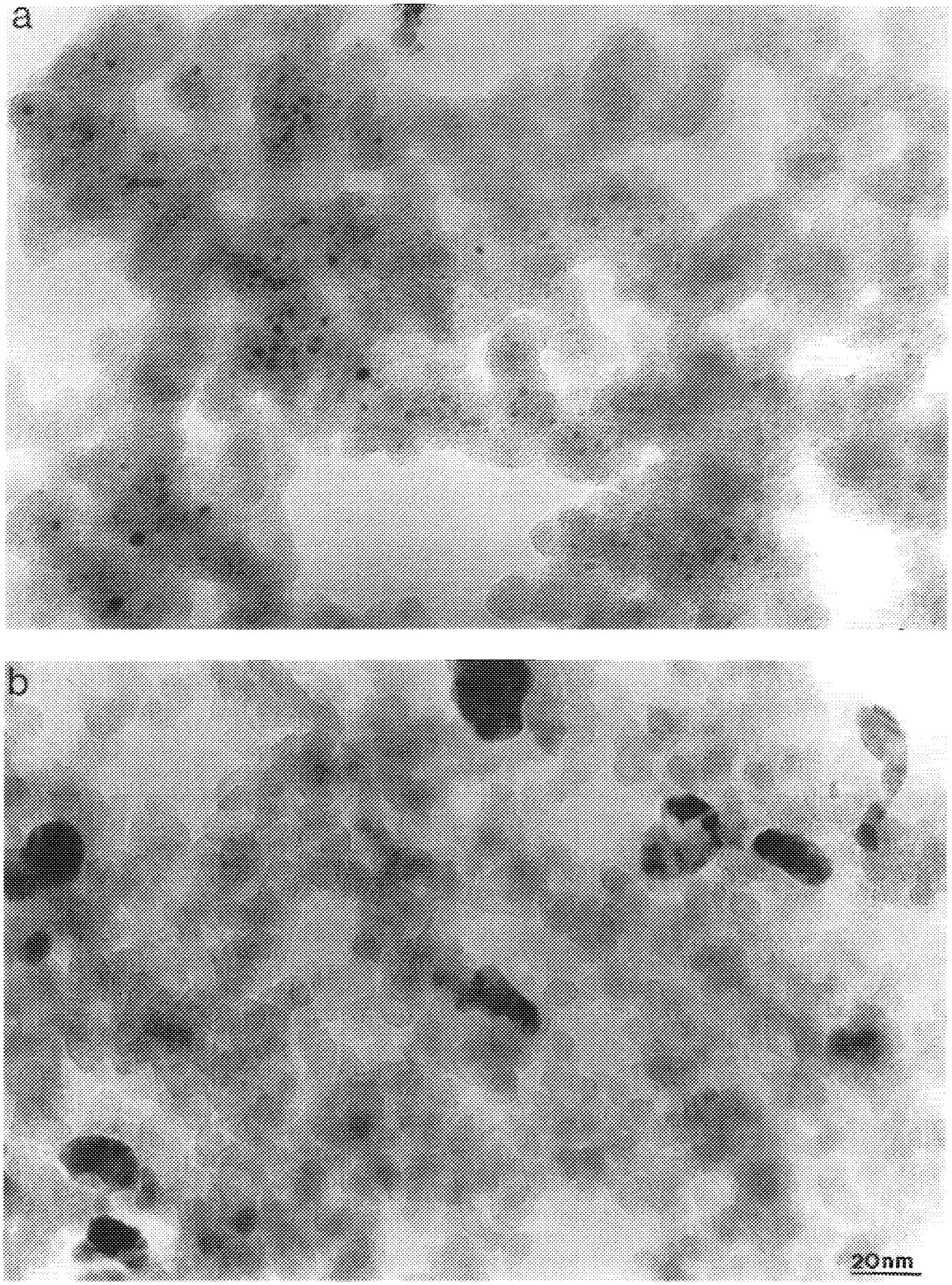

FIG. 10. Transmission electron micrographs of (a) sample Rh/573 and (b) sample Rh/1173 after LT-reduction at 523 K.

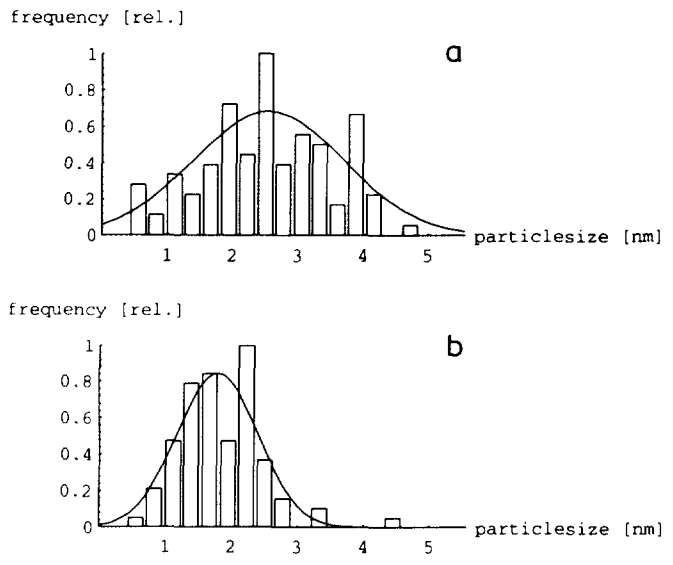

FIG. 11. Particle size distribution for (a) sample Rh/573 after reduction at 523 K (see Fig. 10a) and (b) sample Rh/V/773 after reduction at 523 K (see Fig. 12b).

although they appear to be less opaque. Also, similarly to the Rh/V/973 reduced at 523 K, these structures are again decorated by large numbers of small Rh° metal particles in the size range between 0.7 and 1.4 nm. These are frequently aligned in parallel chains. Hence, Rh/V/1173 when reduced at 773 K leads to morphologies and particles similar to those obtained for Rh/V/973 when reduced at 523 K. The highly dispersed Rh° particles are preferentially located on a V_2O_3 matrix which results from (partial) reduction of the precursor $RhVO_4$. The micrographs of Figs. 12c and 13b provide the first direct observation of highly dispersed Rh° particles sitting on patches or crystallites of V_2O_3 when vanadia-promoted Rh/SiO_2 catalysts were reduced in H_2.

A model that emerges from the results for the vanadium-containing Rh/SiO_2 catalysts which are calcined at elevated temperatures (namely, 973 and 1173 K) is schematically shown in Fig. 14. In the oxide precursor state, Rh_2O_3, V_2O_5 and $RhVO_4$ are present on the SiO_2 surface. The former two components are relatively highly dispersed, with Rh_2O_3 probably not being very abundant at the V/Rh atomic ratio of 4. The $RhVO_4$ forms well-crystallized rod-like particles when the samples are calcined at 1173 K. In the reduced state, V_2O_3 is formed from V_2O_5 and from $RhVO_4$. The reduction of the latter leads to highly dispersed Rh° metal particles being stabilized on the resulting V_2O_3 matrix.

It is interesting to note that CO chemisorption data are not consistent with the particle sizes measured by TEM and/or XRD. Table 3 summarizes the CO chemisorption results for the four $Rh/V/SiO_2$ samples after both LT- and HT-reduction. The data are presented as the saturation amount of CO chemisorbed in μmol per g catalyst (n), and as the calculated CO/Rh atomic ratio. It is clear from the data presented in Table 3 that, for all samples (except Rh/V/1173), the CO uptake decreases with increasing reduction temperatures as expected. As a consequence, the CO/Rh ratios, and hence, the metal dispersions, formally decrease. The absolute CO uptake values and CO/Rh ratios are unusually low and apparently inconsistent with the particle sizes seen in TEM and measured by XRD (when possible) and they are practically zero for Rh/V/1173 within the sensitivity limits of the experimental procedure. The values fall well into the range reported for typical SMSI (strong metal–support interaction) systems (33).

The experimental procedure of pulse CO chemisorption gave reasonable and reproducible data. This has been tested by measuring the CO uptake on Rh/773 reduced at 473 K. A CO/Rh ratio of 0.56 was obtained in this case which compares reasonably well with the particle size range between 1 and 4 nm as seen in TEM. A possible reason for low CO/Rh ratios might be incomplete reduction. However, previous TPR results (22) have shown that Rh/V/573 and Rh/V/773 are completely reduced at temperatures below 523 K (LTR conditions). Rh/V/1173 is not reduced at all and Rh/V/973 is not fully reduced under these conditions, while reduction at 773 K (HTR conditions) leads to a fully reduced material. Even in Rh/V/1173, the rhodium must be completely reduced to Rh° metal under HTR conditions. Hence, incomplete reduction can hardly account for the low CO/Rh ratios measured, despite the high Rh° dispersions seen in the electron micrographs. The fact that finite though very low CO chemisorption was observed on Rh/V/973 after HTR must be due to the presence of some Rh_2O_3 in the oxide precursor besides $RhVO_4$.

A possible explanation for this apparent discrepancy might be inaccessibility of Rh° surface atoms for CO due to encapsulation and/or surface blocking by VO_x species.

TABLE 3

CO Chemisorption Data for $Rh/V/SiO_2$ Catalysts for LT- and HT-Reduction Conditions

	T_{calc} (K)							
	573		773		973		1173	
T_{red} (K)	n^a	CO/Rh	n	CO/Rh	n	CO/Rh	n	CO/Rh
523	156	0.49	71	0.22	7	0.02	n.d.[b]	n.d.
773	38	0.12	19	0.06	6	0.02	n.d.	n.d.

[a] CO uptake in μmol CO per g catalyst.
[b] n.d., not detectable.

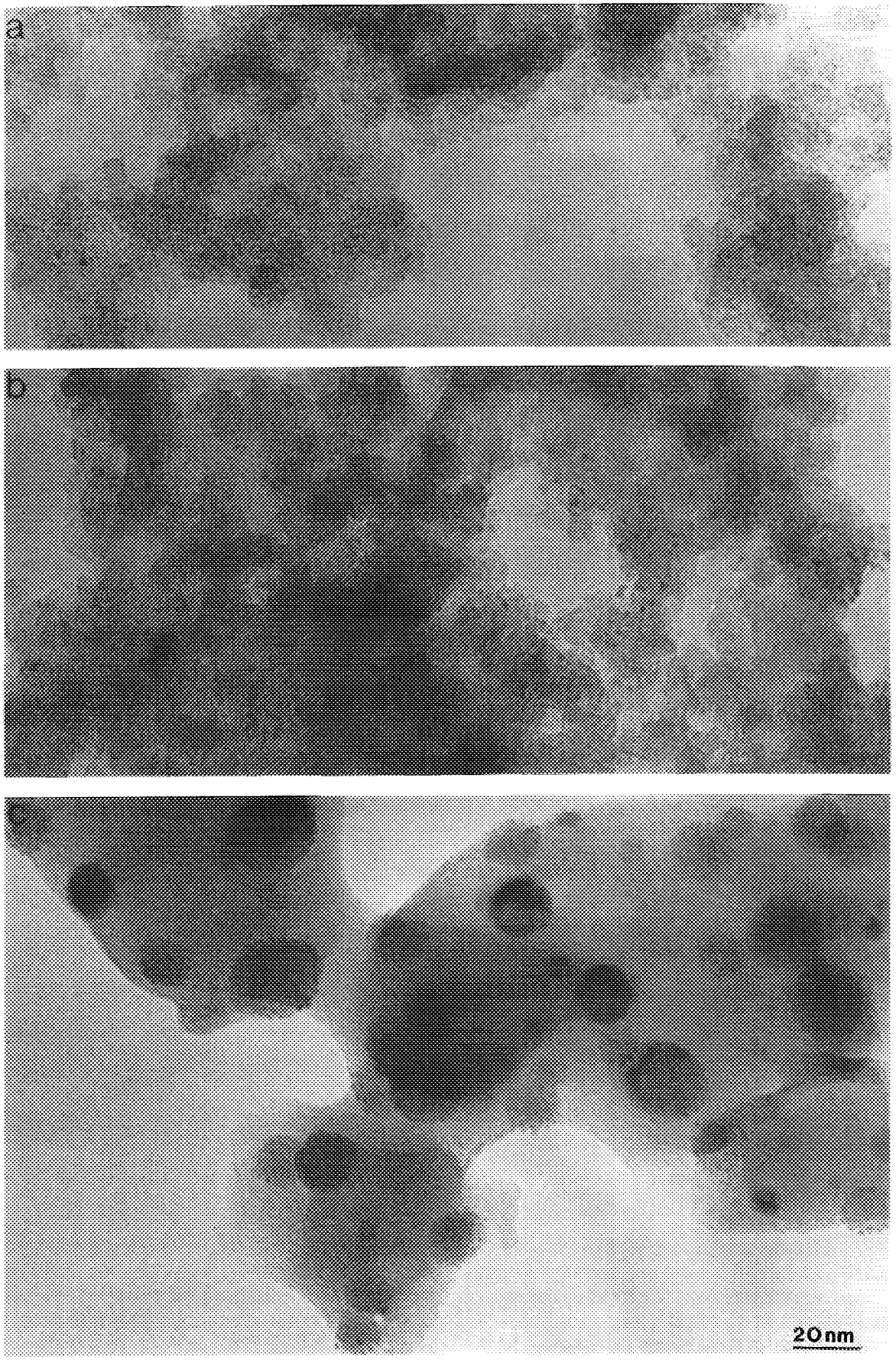

FIG. 12. Transmission electron micrographs of (a) sample Rh/V/573, (b) sample Rh/V/773, and (c) sample Rh/V/973 after LT-reduction at 523 K.

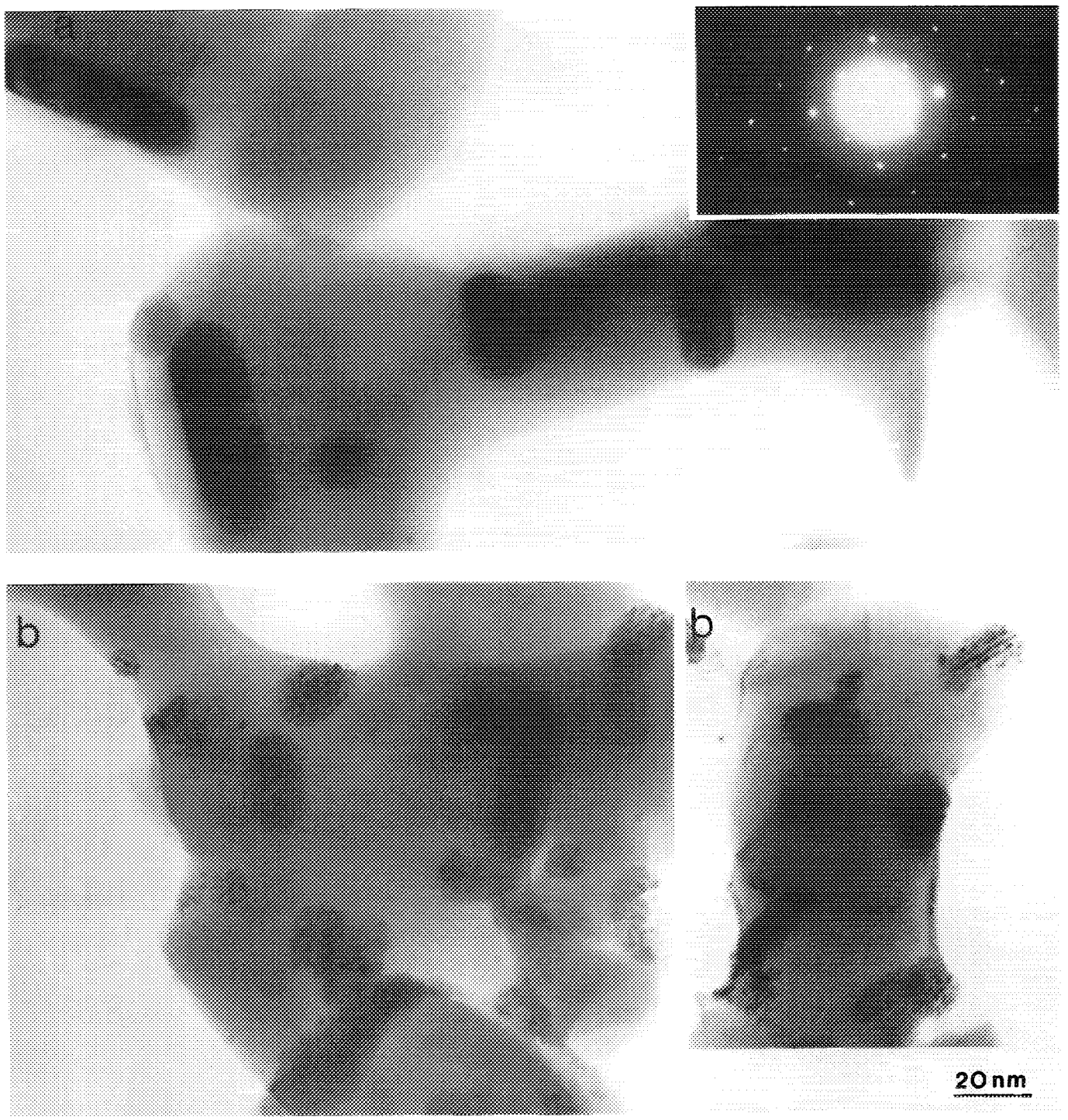

FIG. 13. Transmission electron micrographs of sample Rh/V/1173 (a) after LT-reduction at 523 K and (b) after HT-reduction at 773 K.

This assumption should be reasonable when the materials were reduced under HTR conditions and/or when the oxide precursor was the ternary oxide $RhVO_4$, since vanadium oxide is known as an SMSI support (or promoter) (33). However, in the present series of samples, Rh/V/573 and Rh/V/773 also give very low CO/Rh ratios when reduced at only 523 K, suggesting that surface blocking has occurred even under LTR conditions for these preparations. The same observation had been made by Kip *et al.* (21).

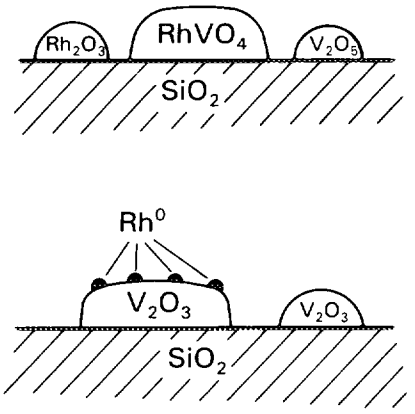

FIG. 14. Model structures of Rh/V-catalysts in the oxide state (top) and after reduction (bottom).

The morphology model shown in Fig. 14 has to be modified accordingly. The small metal particles indicated for the reduced sample must be largely covered by VO_x species consistent with the suggestions of Kip *et al.* (21) and of Hu *et al.* (9).

4. CONCLUSIONS

The present TEM results are fully consistent with previous characterizations of Rh/SiO_2 catalysts promoted by vanadium oxide and they provide the first direct observation of the structure evolutions and morphologies of the various components in this catalyst system upon calcination and reduction. In particular it could be demonstrated that the ternary oxide $RhVO_4$ is formed at elevated calcination temperatures ≥973 K. Well-crystallized, rod-like particles of $RhVO_4$ are detected after calcination at 1173 K. While the materials are easily reducible at 523 K in flowing H_2, the latter sample is only reduced at 773 K. Very high metal dispersions are stabilized by the interaction of Rh with the promoter oxide V_2O_3 which forms upon reduction, as judged from particle size distributions which were obtained from electron micrographs. However, at least for the materials calcined at 773 K and higher temperatures, the experimental CO/Rh ratios were unexpectedly low, suggesting that the Rh° metal surface was decorated and blocked by VO_x. This effect was more pronounced in the materials calcined at higher temperatures and for a given calcination temperature it increased with increasing reduction temperature. An exception to these trends was Rh/V/1173, which did not reduce at low temperature and in which Rh° particles were apparently totally encapsulated after reduction at 773 K. It should be emphasized that the surface blocking, although enhanced with increasing reduction temperature, did in fact occur at low reduction temperature in the present system.

Very similar behaviour was found for niobium- and tantalum-oxide-promoted Rh/SiO_2 catalysts. Characterization data of these systems and the effects of the morphology and structure of the catalysts on their catalytic properties in CO + H_2 reactions will be reported separately.

ACKNOWLEDGMENTS

This work was financially supported by the Deutsche Forschungsgemeinschaft (SFB 338), the Bundesminister für Forschung und Technologie, and the Fonds der Chemischen Industrie. The authors wish to thank Professor H.-P. Boehm for providing the facilities for CO chemisorption measurements, and Dr. H. E. Göbel for the XRD measurements. We also thank Mrs. U. Klengler and Mrs. G. Weinberg for the assistance with the electron microscopy.

REFERENCES

1. Ichikawa, M., Shikakura, K., and Hawai, M., *in* "Proc. Symp. Heterogeneous Catalysis Related to Energy Problems," Dalian, P. R. China, 1982, paper A 08 J.
2. van der Lee, G., Schuller, L., Post, H., Favre, T. L. F., and Ponec, V., *J. Catal.* **98,** 522 (1986).
3. van der Lee, G., Bastein, A. G. T. M., van den Boogert, J., Schuller, B., Luo, H.-Y., and Ponec, V., *J. Chem. Soc. Faraday Trans. 1* **83,** 1893 (1987).
4. Luo, H.-Y., Bastein, A. G. T. M., Mulder, A. A. J. P., and Ponec, V., *Appl. Catal.* **38,** 241 (1988).
5. Kip, B. J., Smeets, P. A. T., van Grondelle, J., and Prins, R., *Appl. Catal.* **33,** 181 (1987).
6. Kip, B. J., Hermanns, E. G. F., and Prins, R., *Appl. Catal.* **35,** 141 (1987).
7. Sachtler, W. M. H., and Ichikawa, M., *J. Phys. Chem.* **90,** 4752 (1986).
8. van den Berg, F. G. A., Glezer, J. H. E., and Sachtler, W. M. H. *J. Catal.* **93,** 340 (1985).
9. Hu, Z., Wakasugi, T., Maeda, A., Kunimori, K., and Uchijima, T., *J. Catal.* **127,** 276 (1991).
10. Mori, T., Miyamoto, A., Takahashi, N., Fukagaya, M., Hattori, T., and Murakami, Y., *J. Phys. Chem.* **90,** 5197 (1986).
11. Ren-Hu, Wang, and Yin Sheng, Xu, *J. Mol. Catal.* **54,** 478 (1989).
12. Underwood, R. P., and Bell, A. T., *J. Catal.* **109,** 61 (1988).
13. Nonnemann, L. E. Y., and Ponec, V., *Catal. Lett.* **7,** 197 (1990).
14. Lavalley, J. C., Saussey, J., Lamotte, J., Breault, R., Hindermann, J. B., and Kiennemann, A., *J. Phys. Chem.* **94,** 5941 (1990).
15. Kiennemann, A., Breault, R., Hindermann, J.-P., and Laurin, M., *J. Chem. Soc. Faraday Trans.* **83,** 2119 (1987).
16. Koerts, T., Welters, W. J. J., van Santen, R. A., Nonnemann, L. E. Y., and Ponec, V., *Stud. Surf. Sci.* **61,** 235 (1991).
17. Knözinger, H., *in* "Homogeneous and Heterogeneous Catalysis" (Yu. I. Yermakov and V. Likholobov, Eds.), p. 789. VNU Press, Utrecht, 1986.
18. Hindermann, J. P., Hutchings, G. J., and Kiennemann, A., *Catal. Rev.—Sci. Eng.* **35,** 1 (1993).
19. Yermakov, Yu. I., Ryndin, Yu. A., Alekseev, O. S., Zaikovskii, V. I., and Pashis, A. V., *Appl. Catal.* **26,** 131 (1986).
20. Trunschke, A., Ewald, H., Gutschick, D., Miessner, H., Skupin, M., Walter, B., and Bloettcher, H.-C., *J. Mol. Catal.* **56,** 95 (1989).
21. Kip, B. J., Smeets, P. A. T., van Wolput, J. H. M. C., Zandbergen, H. W., van Grondelle, J., and Prins, R., *Appl. Catal.* **23,** 157 (1987).
22. Beutel, T., Knözinger, H., Siborov, A. V., and Zaikovskii, V. I., *J. Chem. Soc. Faraday Trans.* **88,** 2775 (1992).

23. Lapina, O. B., Mastikhin, V. M., Nosov, A. V., Beutel, T., and Knözinger, H., *Catal. Lett.* **13,** 203 (1992).
24. Shapligin, I. S., Prosychev, I. I., and Lazarev, V. B., *Russ. J. Inorg. Chem.* **23,** 773 (1978).
25. Vernoni, L. W., and Milligan, W. O., *Texas J. Sci.* **3,** 82 (1951).
26. Kunimori, K., Hu, Z., Uchijima, T., Asakura, K., Iwasawa, Y., and Soma, M., *Catal. Today* **8,** 85 (1990).
27. Hu, Z., Nakamura, H., Kunimori, K., Asano, H., and Uchijima, T., *J. Catal.* **112,** 478 (1988).
28. Legrouri, A., Baird, T., and Fryer, J. R., *J. Catal.* **140,** 173 (1993).
29. del Arco, M., Holgado, M. J., Martin, C., and Rives, V., *Langmuir* **6,** 801 (1990).
30. Yates, D. J. C., and Sinfelt, J. H., *J. Catal.* **8,** 348 (1967).
31. Duprez, D., Barrault, J., and Geron, G., *Appl. Catal.* **37,** 105 (1988).
32. Chen, M., Wang, T., and Schmidt, L. D., *J. Catal.* **60,** 356 (1979).
33. Bond, G. C., and Burch, R., *in* "Catalysis, Vol. 6" (G. C. Bond and G. Webb, Eds.), p. 27. The Royal Society of Chemistry, London, 1983.